Available online at www.sciencedirect.com
ScienceDirect
Journal of Power Sources 175 (2008) 613–620
JOURNAL OF POWER SOURCES
www.elsevier.com/locate/jpowsour

A novel electrode-bipolar plate assembly for vanadium redox flow battery applications

Peng Qian [a,b], Huamin Zhang [a,*], Jian Chen [a], Yuehua Wen [a], Qingtao Luo [a,b], Zonghao Liu [a], Dongjiang You [a,b], Baolian Yi [a]

[a] *Lab of PEMFC Key Materials and Technologies, Dalian Institute of Chemical Physics, Chinese Academy of Sciences, Dalian, Liaoning 116023, China*
[b] *Graduate School of the Chinese Academy of Sciences, Beijing 100039, China*

Received 13 August 2007; received in revised form 4 September 2007; accepted 4 September 2007
Available online 11 September 2007

Abstract

A novel electrode-bipolar plate assembly has been developed and evaluated for application in the vanadium redox flow battery (VRB). It is composed of three parts: a graphite felt (electrode), an adhesive conducting layer (ACL) and a flexible graphite plate (bipolar plate). The ACL connects the electrode with the bipolar plate to an assembly. By the evaluations of cost, resistivity, surface morphology, electrolyte permeation and single cell performance, this novel assembly demonstrates its applicability in VRB as evident in the following outcomes: (1) lowers the cost and area resistivity to about 10% and 40% of the conventional setups, respectively; (2) improves electrical conductivity to 4.97 mΩ cm as compared to over 100 mΩ cm of the carbon-plastic composite bipolar plate; (3) attains zero electrolyte permeation; and (4) achieves a higher energy efficiency of 81% at a charge/discharge current density of 40 mA cm^{-2} when employed in a VRB single cell, which is 73% for the conventional setup. All these indicate that the novel electrode-bipolar plate assembly is a promising candidate for VRB applications.

Keywords: Flexible graphite; Adhesive conducting layer; Electrode-bipolar plate setup; Vanadium redox flow battery; Energy storage

1. Introduction

The redox flow battery is an electrochemical device for energy storage, which was first proposed by Thaller in 1975 [1]. Redox flow batteries based on iron/chromium, bromine/polysulphide, vanadium/bromine, zinc/bromine, zinc/cerium, and vanadium redox couples were developed in subsequent research investigations. Among these promising candidates, the vanadium redox flow battery (VRB) showed great potential for commercialization. In the VRB system, the VO^{2+}/VO_2^+ and V^{3+}/V^{2+} redox couples are employed for the positive and negative half-cells, respectively. The half-cell reactions are as follows:

$$\text{Positive half-cell}: VO^{2+} + H_2O - e^- \underset{\text{Discharge}}{\overset{\text{Charge}}{\rightleftarrows}} VO_2^+ + 2H^+,\ E^0 = +1.00\ V \text{ versus SHE};$$

$$\text{Negative half-cell}: V^{3+} + e^- \underset{\text{Discharge}}{\overset{\text{Charge}}{\rightleftarrows}} V^{2+},\ E^0 = -0.26\ \text{V versus SHE}.$$

(Using 1 mol dm^{-3} concentrations at 25 °C, the standard open circuit cell potential of the VRB system is 1.26 V [2]).

In the VRB system, all the reactants and products of the electrode reactions remain dissolved in either of the two electrolytes. In case solution crossover occurs, the vanadium half-cell electrolytes can be remixed, and the system can be brought back to its original state, albeit with energy efficiency loss [2]. The output power is determined by the number of cells and the surface areas of the electrodes, while the energy storage capacity is determined by the concentration and the volume of the electrolyte. Therefore, the output power and the energy storage capacity of the VRB system are independent. Furthermore, low cost carbon-plastic materials can be applied for VRB components (electrodes and bipolar plates). With these specific properties, VRB certainly gains consid-

* Corresponding author. Tel.: +86 411 8437 9072; fax: +86 411 84665057.
E-mail address: zhanghm@dicp.ac.cn (H. Zhang).

0378-7753/$ – see front matter © 2007 Elsevier B.V. All rights reserved.
doi:10.1016/j.jpowsour.2007.09.006

erable advantages over conventional energy storage systems [3–10].

The relatively fast kinetics of vanadium redox couples allow high coulombic and voltage efficiencies to be obtained, but the values of these efficiencies also depend on the internal ohmic resistance (IOR) of VRB. Electrodes and bipolar plates are the key components of VRB. The performance of the battery depends strongly on the bulk resistivities of the electrode, the bipolar plate and the contact resistance between them (main contributor to the IOR of VRB). Generally, graphite felts and impermeable graphite plates serve as the electrodes and bipolar plates, respectively, in VRB. The conventional electrode-bipolar plate setup is comprised of pressed-contacted graphite felts on impermeable graphite plates (i.e., the graphite felt electrode comes into contact with the impermeable graphite bipolar plate by assembly compact force). In this case, if the assembly compact force is too high, the graphite felt electrode will be compressed heavily, which results in high electrolyte flow resistance. However, if the assembly compact force is too weak, the contact resistance between the graphite felt electrode and the bipolar plate will be large. In addition, the impermeable graphite bipolar plate is expensive and brittle, which also limits its practical application. Thus, carbon-plastic composite electrodes were put forward in the 1980s [11]. In such structures, the graphite felts are heat bonded to the conductive carbon-plastic composite bipolar plates. As compared to the conventional electrode-bipolar plate setup, such carbon-plastic composite electrodes are cheap, flexible and lightweight. Moreover, the penetration of graphite felt fibers into the conductive carbon-plastic composite bipolar plate during the heat bonding process leads to an increase in the contact points of the graphite felt fibers with the bipolar plate. As a result, low contact resistances between graphite felt electrodes and bipolar plates can be achieved for the carbon-plastic composite electrodes even under a small assembly compact force. Because of these benefits, more and more research has focused on the design and manufacture of carbon-plastic composite electrodes and their related materials [12–19]. In 2002, a new carbon-plastic composite electrode was reported, which reduced the processing time and cost. This novel approach was characterized by using a completely nonconductive polymer sheet material (high-density polyethylene or low-density polyethylene) with melt flow properties. These facilitate the high penetration of carbon graphite felt fibers and the interconnection of such fibers during the heat bonding process [20]. However, the conductivity of the carbon-plastic composite electrode is much less than that of graphite material. Generally, the bulk resistivities of these carbon-plastic composite materials are over 100 mΩ cm, while for graphite material, less than 10 mΩ cm can be achieved [21].

Combining the high bulk conductivities of graphite materials with the advantages of carbon-plastic composite electrodes, a novel electrode-bipolar plate assembly was developed in our lab. A flexible graphite plate served as the bipolar plate, and a thin adhesive conducting layer (ACL) was prepared on the surface of the flexible graphite bipolar plate. Finally, the graphite felt electrode was heat bonded to the flexible graphite bipolar plate with ACL. The sketch of the novel electrode-bipolar plate assembly is presented in Fig. 1.

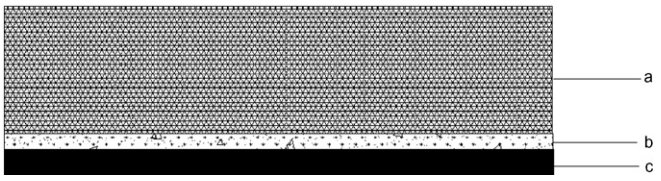

Fig. 1. Sketch of the novel electrode-bipolar plate assembly (cross-sectional view): (a) graphite felt; (b) ACL; (c) flexible graphite bipolar plate.

Flexible graphite, such as that developed in this work, can alleviate some of the concerns related to weight, cost and conductivity of VRB. Conventional impermeable graphite bipolar plates contribute significantly to the cost and weight of VRB stacks. Carbon-plastic composite materials are favored for their low cost, but they are not advisable to use because of conductivity-related issues. The cost, weight and resistivity of flexible graphite, impermeable graphite and carbon-plastic composite materials are compared and shown in Table 1 [22–26]. As compared to impermeable graphite and carbon-plastic composite materials, the economic and physical attributes of flexible graphite make it a more promising material for VRB applications. Moreover, its good flexural property assists in preventing cracking during the cell assembly process. However, there are limited studies to date concerning the application of flexible graphite in VRB. In this work, flexible graphite plate is used as the bipolar plate (acts as current collector and ACL support).

In addition, it is worth noting that ACL plays a vital role in our novel electrode-bipolar plate assembly. It is composed of thermo-plastic phenol formaldehyde resin (PF), carbon black and graphite powder. ACL is a carbon-plastic composite layer, but it is much thinner than the carbon-plastic composite bipolar plate. As a result, as compared to carbon-plastic composite bipolar plates, low bulk resistivity can be achieved for a flexible graphite bipolar plate with ACL. Furthermore, as compared to the conventional electrode-bipolar plate setup, the penetration of graphite felt fibers into ACL occurs during the heat bonding process. This is similar to the process of carbon-plastic composite electrode preparation and is due to the thermal viscosity of ACL (PF resin cure at 150 °C). Therefore, low contact resistance between the electrode and the bipolar plate can be achieved for the novel electrode-bipolar plate assembly under small assembly compact force. Moreover, ACL can also prevent electrolyte from infiltrating through the flexible graphite plate (vanadium

Table 1
Comparison of the economic and physical properties of different bipolar plate materials

Material	Material cost (US$ kg^{-1})	Bulk resistivity (mΩ cm)	Density (g cm^{-3})
Flexible graphite	4–5	3.8	1.00
Impermeable graphite	75	1.0	1.98
Carbon-plastic composite material [21,25,26]	5–30	>100.0	>1.30

ions can penetrate through the flexible graphite after soaking for a long time in electrolyte).

In this work, the novel electrode-bipolar plate assembly described above was developed and applied for a VRB single cell. Correspondingly, its bulk resistivity, area resistance, morphology of ACL, electrolyte permeability, and single cell performance were investigated.

2. Experimental

2.1. Preparation of the adhesive conducting material (ACM, material for ACL preparation) and the novel electrode-bipolar plate assembly

The materials employed for ACM preparation include the following: (a) thermo-plastic phenol formaldehyde resin (PF) (Tianjin resin factory); (b) hexamethylene tetramine (Shenyang fifth reagent factory); (c) graphite powder (Shanghai colloid chemical plant); and (d) carbon black (Vulcan® XC-72 R, Cabot). To prepare ACM, the above materials were mixed together with a weight ratio of a:b:c:d = 2:0.2:1:1. A ball-mill process followed in which agate jar and balls were used. The rotation rate and time were 500 revolutions per minute and 5 h, respectively.

After adding ethanol (Concord Technology Co Ltd.), ACM was dispersed sufficiently in an ultrasonic bath for 15 min. Then the mixture was poured into a steel mold frame with inner dimensions of 25 mm × 20 mm, which was already set on the surface of the flexible graphite bipolar plate (Cathay Packing & Sealing Co Ltd.). After the ethanol was completely evaporated at 60 °C, ACL was obtained. The thickness of ACL was controlled by the loading of ACM on the bipolar plate. To prepare the novel electrode-bipolar plate assembly, the graphite felt sheet with a dimension of 25 mm × 20 mm × 4.6 mm was heat bonded to the flexible graphite bipolar plate with ACL at 150 °C for 30 min.

2.2. Bulk resistivities measurement

The bulk resistivities of the flexible graphite bipolar plate, flexible graphite bipolar plate with ACL and graphite felt were measured. Digital four-probe bulk resistivity measurement equipment (SX1934, Baishen Technology) was employed. The four-point probe has a linear configuration with spacing of 1 mm between the probes. The samples were with the dimension of 2 cm × 2 cm.

2.3. Area resistance measurement

The area resistance R_a was defined as $R_a = R_t \times A$, where R_t was the resistance in the through-plane direction (including the resistance of the electrode, bipolar plate, and the contact resistance between them; here, the contact resistance between the sample and the talmigold plates was ignored), and A was the area of the sample. Fig. 2 presents a schematic illustration of the experimental setup applied to measure area resistance. The method basically involved measuring the potential difference across two talmigold plates, which sandwiched the sample, as a constant electrical current was passed through them. The variation in potential difference was recorded as the compaction force applied to the assembly was gradually increased. By measuring the voltage drop, it was possible to calculate the resistance in the through-plane direction, that is, $R_t = V/I$. The area resistance of the conventional electrode-bipolar plate setup and the novel electrode-bipolar plate assembly with different ACM loading were measured with the same procedure. The area of the test sample was 20 cm^2. The compact pressure applied increased from 5 to 70 N cm^{-2}.

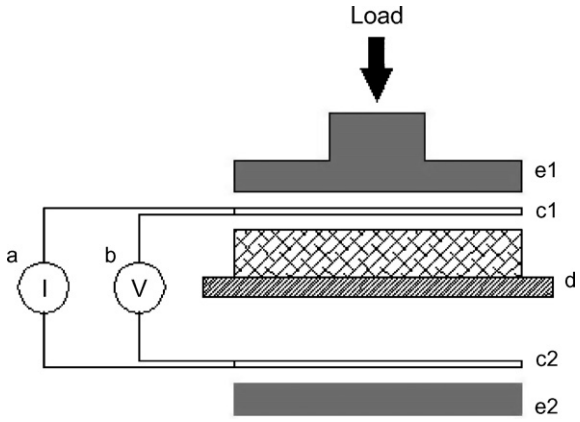

Fig. 2. Schematic diagram of the experimental setup for measuring area resistance. (a) Invariable electrical current source and current meter; (b) voltage meter; (c1, c2) talmigold plate; (d) sample; (e1, e2) compact force machine.

2.4. Surface morphology of ACM and ACL

The morphology of the ACM particles (before cure) and the ACL (after cure) were observed with SEM (JSM-6360LV, JEOL).

2.5. Permeability measurement

Flexible graphite bipolar plates with and without ACL (on both sides) were assembled in a flow cell, where 30 ml 1.5 M VO^{2+} in 3M H_2SO_4 solution was pumped through on one side and 30 ml distilled water was pumped on the other side for 500 h. In the distilled waterside, the amount of VO^{2+} ions penetrated through the bipolar plate was detected with UV–vis spectroscopy (UV-4802, Unico).

2.6. Performance of VRB single cells

Fig. 3 is the configuration of a lab-scale VRB single cell experimental set-up. The end plates were made of stainless steel, while the gaskets and frames were made of fluoroelastomer. The tie-ins and pipelines were all made of polytetrafluoroethylene. During the operation of the cell, the anolyte and catholyte were pumped through their own chamber and then flew back into two separated tanks.

The cell charge and discharge cycles were controlled automatically and continuously by a custom-designed multi-channel battery testing system (CT2001A, Land) between the set upper

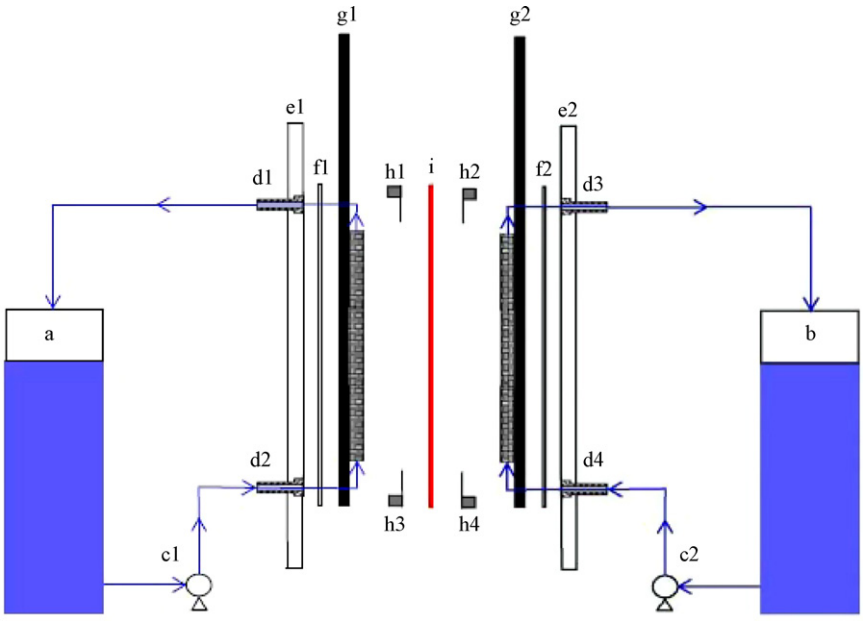

Fig. 3. The structure diagram of a VRB single cell: (a) positive electrolyte tank; (b) negative electrolyte tank; (c1, c2) magnetic pump; (d1, d2, d3, d4) tie-in; (e1, e2) end plate; (f1, f2) gasket; (g1, g2) electrode and bipolar plate; (h1, h2, h3, h4) electrode frame; (i) cation exchange membrane.

charge voltage limit of 1.75 V and lower voltage limit of 0.8 V. During charge–discharge tests, the voltages of the cell were measured and recorded at a fixed interval of 5 s. The cell coulombic efficiency (CE) was defined as the discharge capacity divided by the charge capacity; the energy efficiency (EE) was defined as the discharge energy divided by the charge energy. Then the voltage efficiency (VE) was calculated from VE = EE/CE.

2.7. Operating conditions of the experiments

The operating conditions were as follows:

- The cure condition of ACM and ACL for SEM and the permeability of the electrolyte test was 150 °C for 30 min.
- Initial positive side: 60 ml 1.5 M $VOSO_4$ + 3 M H_2SO_4 solution.
- Initial negative side: 30 ml 1.5 M $VOSO_4$ + 3 M H_2SO_4 solution.
- Both of the negative and positive electrode areas were 5 cm^2 in geometric area.
- The flow rates of the two electrolytes were both about 30 ml min^{-1}.
- A sheet of Nafion® 117 membrane was used as separator.
- All experiments were carried out at room temperature.

Each electrolyte compartment contained 30 ml of electrolyte, except for the initial charging of the cell where twice as much electrolyte (60 ml) was required in the positive compartment. After the first charging, half of the electrolyte in the positive compartment was removed.

3. Results and discussion

3.1. Bulk resistivities of materials for the novel electrode-bipolar plate assembly

To evaluate the effect of ACL on the conductivity of the novel electrode-bipolar plate assembly, the bulk resistivities of the flexible graphite bipolar plate, flexible graphite bipolar plate with ACL (after cure), and graphite felt were measured, and the results are shown in Table 2. It can be seen that the bulk resistivity of graphite felt is over seven times greater than that of the other two parts, indicating that graphite felt is the main contributor to the bulk resistivity of the novel electrode-bipolar plate assembly. This can be attributed to the porous structure of the graphite felt. In addition, comparing flexible graphite bipolar plates with and without ACL, it is found that the bulk resistivity of the former is not significantly higher than that of the latter despite the addition of a certain amount of nonconductive polymer in ACL. This indicates that the addition of ACL on flexible graphite bipolar plates does not lead to a rapid increase in bulk resistivity. Furthermore, the bulk resistivity of a flexible graphite bipolar plate

Table 2
Bulk resistivity of flexible graphite bipolar plate, flexible graphite bipolar plate with ACL (after cure), and graphite felt

Sample	Bulk resistivity (mΩ cm)	Thickness (mm)
Graphite felt	35.00	4.6
Flexible graphite bipolar plate	3.80	2.3
Flexible graphite bipolar plate with ACL (after cure)	4.97	2.5

with ACL is more acceptable than that (over 100 mΩ cm) of a carbon-plastic composite electrode.

3.2. Area resistance comparison for the conventional electrode-bipolar plate setup and the novel electrode-bipolar plate assembly

Low resistance is essential to the electrode-bipolar plate setup, especially in the through-plane direction. Here, area resistance (defined in Section 2.3) is used to assess the resistance of the electrode-bipolar plate setup in the through-plane direction. The conventional electrode-bipolar plate setup gives a high area resistance with a small compact pressure applied; in comparison, over-compression may lead to poor electrolyte transport and the possibility of graphite felt damage. One of the objectives of this work was to prepare a novel electrode-bipolar plate assembly with a lower area resistance and with less compression. Fig. 4 shows the comparison of the area resistance of the conventional electrode-bipolar plate setup and that of the novel electrode-bipolar plate assembly. As can be seen, the area resistance of the novel electrode-bipolar plate assembly is lower than that of the conventional electrode-bipolar plate setup on the whole (especially at a low compact pressure). With an increase in compact pressure, the area resistance decreases rapidly at first and gradually later for both electrode-bipolar plate setups. For the conventional electrode-bipolar plate setup, there are two reasons for the decrease in area resistance. The first is the decrease in porosity of the graphite felt and the increase in fiber–fiber contact points with compact pressure clamped. As a result, the increase in the number of contact points leads to more electron passages available, which in turn brings about a fast decrease in area resistance. The second is the increase in electrode-bipolar plate contact points with compact pressure clamped, and more extra electron passages are achieved. However, for the novel electrode-bipolar plate assembly, the graphite felt is bound to the bipolar plate by ACL, which keeps the electrode-bipolar plate contact points fixed. Therefore, the only reason for the decrease in area resistance is the more electron passages opened by the

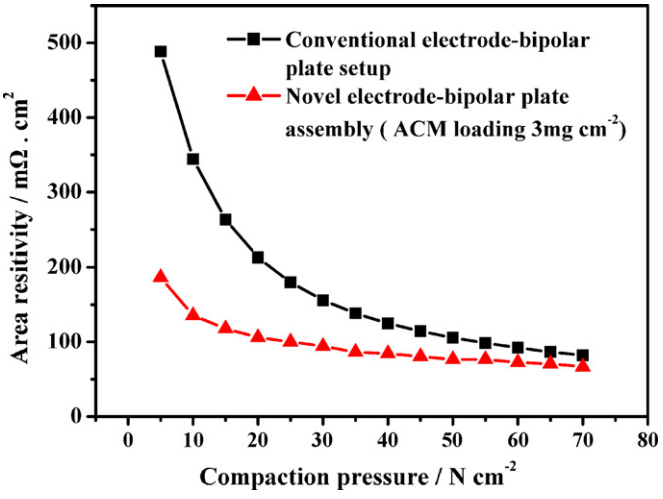

Fig. 4. Comparison of area resistance for the conventional electrode-bipolar plate setup and the novel electrode-bipolar plate assembly.

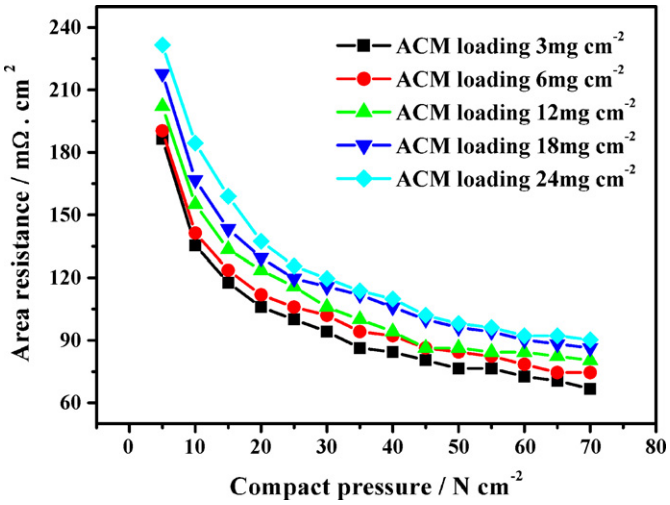

Fig. 5. The area resistances of the novel electrode-bipolar plate assemblies with different ACM loadings.

increase in graphite felt fiber–fiber contact points with compact pressure clamped. As a result, the area resistance of the conventional electrode-bipolar plate setup drops faster than that of the novel electrode-bipolar plate assembly with an increase in compact pressure. Because of the roothold of ACL, the number of electrode-bipolar plate contact points of the novel electrode-bipolar plate assembly is larger than that of the conventional electrode-bipolar plate setup. As a result, the area resistance of the composite electrode is smaller than that of the conventional electrode-bipolar plate setup at a given compact pressure.

3.3. Effect of ACM loading on area resistance

The thickness of ACL is determined by the ACM loading and it affects the area resistance of the novel electrode-bipolar plate assembly. Fig. 5 shows the area resistances of the novel electrode-bipolar plate assemblies with different ACM loadings. It can be seen that there is an increase in area resistance with an increase in ACM loading, and the novel electrode-bipolar plate assembly with an ACM loading of 3 mg cm^{-2} has the lowest area resistance. It is worth noting that in practice, the graphite felt is prone to peel off from the flexible graphite bipolar plate with too little ACM loading (less than 3 mg cm^{-2}). Therefore, 3 mg cm^{-2} is an optimal ACM loading with respect to area resistance for the novel electrode-bipolar plate assembly.

3.4. Morphology of ACM and ACL

The SEM image of ACM (before cure) is shown in Fig. 6(a). The particles can be observed clearly, indicating that they are conductive. Meanwhile, the SEM images of the surface and the cross-section of ACL (after cure) are presented in Fig. 6(b) and (c), respectively. It can be seen clearly from Fig. 6(b) that a unit conductive surface of ACL is formed after cure. Because of the application of the hot-press process, the surface of ACL is compact and level. The thickness of ACL can be estimated from Fig. 6(c) and is about 210 μm.

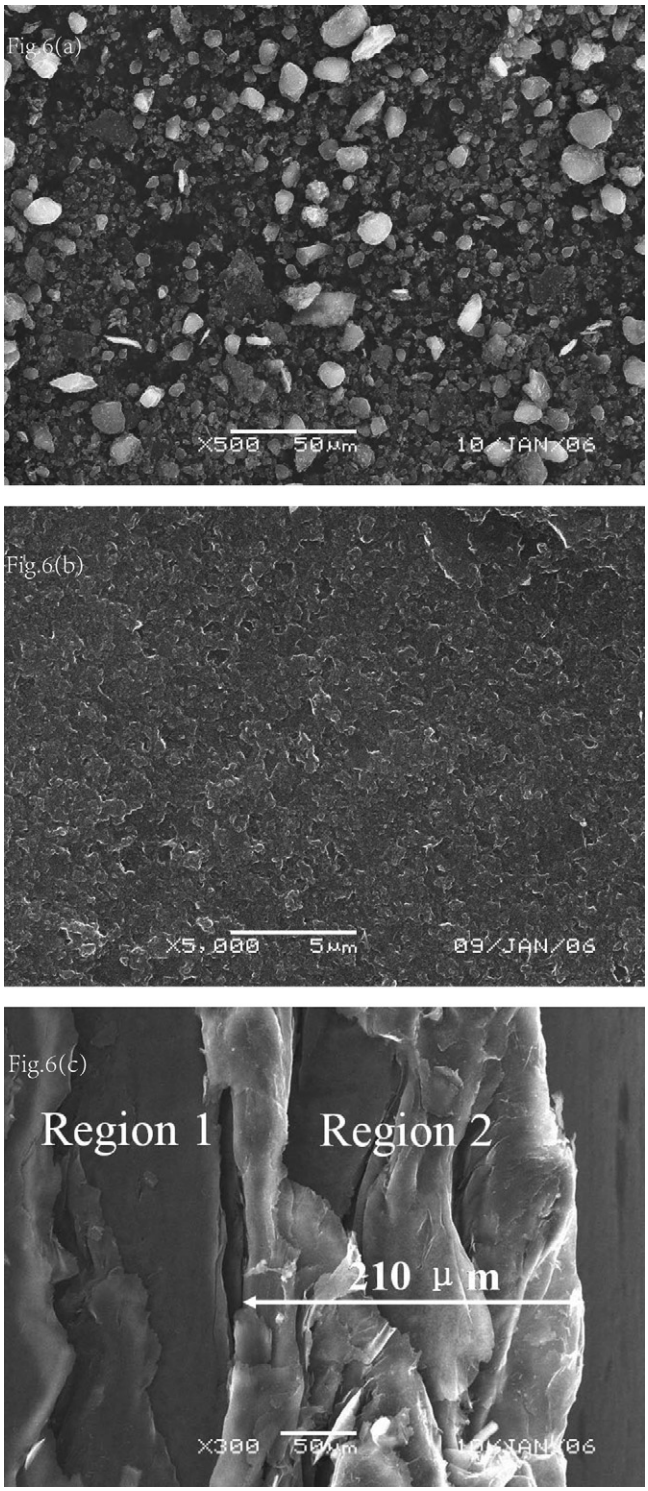

Fig. 6. SEM images of (a) ACM particles (before cure); (b) surface of ACL (after cure); (c) cross-section of ACL. (after cure, Region 1: flexible graphite bipolar plate; Region 2: ACL). Cure condition: 150 °C for 30 min.

3.5. Permeability of the flexible graphite bipolar plate with and without ACL

Electrolyte permeability is one of the most important characteristics of the electrode-bipolar plate setup. As described in Section 2.5, permeability was measured for flexible graphite bipolar plates with and without ACL. For the flexible graphite bipolar plates with ACL, no vanadium ions were detected in the distilled water by UV–vis spectroscopy after operating for 500 h. Without ACL, a vanadium ions concentration of 4.5 mmol l^{-1} was identified on the distilled waterside of the flexible graphite bipolar plate after 500 h. The results indicate that the flexible graphite bipolar plate with ACL can hinder the permeation of the electrolyte efficiently.

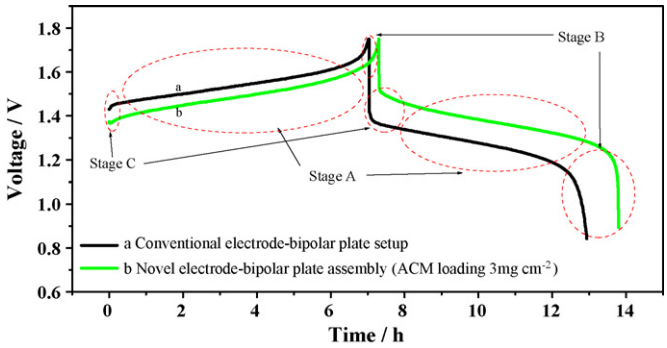

Fig. 7. Typical charge/discharge curves of the single cell with conventional electrode-bipolar plate setup and novel electrode-bipolar plate assembly at a current density of 40 mA cm^{-2}.

3.6. Single cell performance

Single cells (with the conventional electrode-bipolar plate setup and our novel electrode-bipolar plate assembly) at the conditions described in Sections 2.6 and 2.7 (charge/discharge current density was 40 mA cm^{-2}) were run for up to 10 cycles and the typical charge/discharge curves are presented in Fig. 7. Here, we defined three stages as stage A (the stage of charge/discharge), stage B (the stage at the end of charge/discharge) and stage C (the stage at the beginning of charge/discharge). In stage A, the cell's voltage changes smoothly, while stages B and C, the voltage changes sharply. There are various factors affecting the voltage changes of VRB, such as IOR, electrolyte transport, the concentrations of vanadium species in the anolyte and catholyte, the kinetics at both anode and cathode, and the like. In stage A, the changes in the concentrations of vanadium species in the anolyte and catholyte are the main factors that dominate the voltage changes of the cell. This was supported by the gradual color change of the electrolyte, that is, the change in different vanadium species. For example, the colors of the electrolyte for the discharged stage on the positive side varied from yellow (VO_2^+ ions) to blue (VO^{2+} ions), while they varied from purple (V^{2+} ions) to green (V^{3+} ions) on the negative side. This process was moderate. When the cell was charged, the vanadium species and the color of the electrolyte varied in the reverse direction. However, in stage B, concentration polarization led to dramatic voltage decreases at the end of charge/discharge. The IOR dominates the voltage of the cell in stage C [27]. As a result, the cell with smaller IOR exhibits a lower initial charge voltage and a higher initial discharge voltage. The IOR of VRB includes the contact resistance between the electrode and the bipolar plate, the electronic

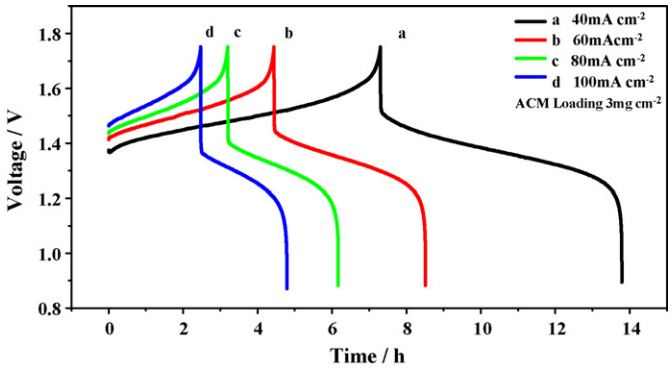

Fig. 8. Typical charge/discharge curves of the single cell with novel electrode-bipolar plate assembly at different current densities.

resistance of the electrode and the bipolar plate, and the ionic resistances of the electrolytes and the ion exchange membrane. The contact resistance between the electrode and the bipolar plate (described by the area resistance defined in Section 2.3) is the main contributor to the IOR. The experimental results in Section 3.2 indicate that the novel electrode-bipolar plate assembly gains an advantage over the conventional electrode-bipolar plate setup in area resistance. When the same electrode, electrolyte and membrane are used, the cell with the novel electrode-bipolar plate assembly presents a lower initial charge voltage and a higher initial discharge voltage than the cell with the conventional electrode-bipolar plate setup. The initial voltage gap between them is about 30 mV. The energy efficiency of 81% was achieved for the novel electrode-bipolar plate assembly, while 73% for the conventional setup.

To evaluate the applicability of the novel electrode-bipolar plate assembly in the VRB single cell, charge/discharge tests at different current densities were carried out as described in Sections 2.6 and 2.7. The typical charge/discharge curves for the novel electrode-bipolar plate assembly are presented in Fig. 8. The efficiencies of the cell were calculated based on the definition in Section 2.6. The values of coulombic efficiency, voltage efficiency and energy efficiency at different current densities are shown in Table 3. It can be seen that the voltage efficiency of 91% and energy efficiency of 81% were achieved for the cell at the current density of 40 mA cm^{-2}. With the increase in current density, the voltage efficiency and energy efficiency decreased to some extent. However, even at a current density of 100 mA cm^{-2}, a voltage efficiency of 82% and an energy efficiency of 77% were still obtained. This indicates the excellent performance of the novel electrode-bipolar plate assembly in VRB applications.

Table 3
Efficiencies of the VRB single cell with the novel electrode-bipolar plate assembly

Current density (mA cm^{-2})	Coulombic efficiency (%)	Voltage efficiency (%)	Energy efficiency (%)
40	89	91	81
60	92	87	80
80	93	85	79
100	94	82	77

3.7. Economic perspectives analysis

Besides material cost (discussed in Section 1), production-related costs such as machinery depreciation, labor, molds and energy consumption, should be taken into consideration. The conventional electrode-bipolar plate setup is characterized by excellent manufacturability due to pressed-contacted graphite felts on impermeable graphite plates. Unfortunately, the high price (75 US$ kg^{-1}) of impermeable graphite counteracts its affordability. To some extent, a similar problem exists in composite electrode fabrication as well. Generally, it is difficult to achieve a price of less than 10 US$ kg^{-1} for carbon-plastic bipolar plates in small-scale production (a number of 5000 plates) [28]. In comparison, flexible graphite with a low price of 5 US$ kg^{-1} is severed as the bipolar plate for the novel electrode-bipolar plate assembly. The amount of ACM per kilogram of flexible graphite bipolar plate (used on both sides) is 30 g with a price of 0.3 US$ (the ACM loading is 3 mg cm^{-2}, the thickness of the flexible graphite bipolar plate is 2 mm with a density of 1.00 g cm^{-3}, and the preparation cost of ACM is 10 US$ kg^{-1}). Including the preparation cost of ACL (2 US$ per kilogram of flexible graphite bipolar plate on both sides), the total cost for the preparation of the flexible graphite bipolar plate with ACL on both sides is estimated to be 7.3 US$ kg^{-1}. As a result, when the same electrode materials are used, the novel electrode-bipolar plate assembly is more competitive in cost than the conventional electrode-bipolar plate setup and the composite electrode.

4. Conclusions

A novel electrode-bipolar plate assembly for VRB applications was proposed and investigated in this paper. Specifically, the application of flexible graphite in the electrode-bipolar plate assembly in this study exceeded many standards set by the industry—for instance, it costs 7.3 US$ kg^{-1}, weighs light at 1.00 g cm^{-3}, and has an acceptable bulk resistivity of 4.97 mΩ cm. Furthermore, it is worth noting that the proposed new structure of the electrode-bipolar plate assembly integrates the electrode with the bipolar plate by ACL. As compared to the conventional electrode-bipolar plate setup, such structure offers almost a 300 mΩ cm^2 drop in area resistivity at 5 N cm^{-2}. No vanadium ions were detected by UV–vis spectroscopy during the 500 h of permeability test, which indicates the impermeability of the novel electrode-bipolar plate assembly. When tested in a VRB single cell, the performance of this novel electrode-bipolar plate assembly achieved an energy efficiency of 81% at a current density of 40 mA cm^{-2}. The single cell charge/discharge cycle test at different current densities with the novel electrode-bipolar plate assembly further demonstrated the assembly's promising application in VRB.

References

[1] L.H. Thaller, US Patent 3,996,064. (1975).
[2] C. Ponce de Léon, A. Frías-Ferrer, J. González-García, D.A. Szánto, F.C. Walsh, J. Power Sources 160 (2006) 716–732.

[3] E. Sum, M. Rychcik, M. Skyllas-Kazacos, J. Power Sources 16 (1985) 85–95.
[4] E. Sum, M. Skyllas-Kazacos, J. Power Sources 15 (1985) 179–190.
[5] M. Skyllas-Kazacos, M. Rychcik, R.G. Robins, et al., J. Electrochem. Soc. 133 (1986) 1057–1058.
[6] M. Rychcik, M. Skyllas-Kazacos, J. Power Sources 19 (1987) 45–54.
[7] M. Skyllas-Kazacos, F. Grossmith, J. Electrochem. Soc. 134 (1987) 2950–2953.
[8] M. Rychcik, M. Skyllas-Kazacos, J. Power Sources 22 (1988) 59–67.
[9] M. Skyllas-Kazacos, R.G. Robins, US Patent 4,786,567 (1986).
[10] M. Skyllas-Kazacos, D. Kasherman, R. Hong, M. Kazacos, J. Power Sources 35 (1991) 399–404.
[11] M. Kazacos, M. Skyllas-Kazacos, J. Electrochem. Soc. 136 (1989) 2759–2760.
[12] S. Zhong, M. Kazacos, R.P. Burford, et al., J. Power Sources 36 (1991) 29–43.
[13] S. Zhong, M. Skyllas-Kazacos, J. Power Sources 39 (1992) 1–9.
[14] V. Haddadi-Asl, M. Kazacos, M. Skyllas-Kazacos, J. Appl. Electrochem. 25 (1995) 29–33.
[15] B.T. Sun, M. Skyllas-Kazacos, Electrochim. Acta 36 (1991) 513–517.
[16] B.T. Sun, M. Skyllas-Kazacos, Electrochim. Acta 37 (1992) 1253–1269.
[17] B.T. Sun, M. Skyllas-Kazacos, Electrochim. Acta 37 (1992) 2459–2465.
[18] V. Haddadi-Asl, M. Kazacos, M. Skyllas-Kazacos, US Patent 5,665,212 (1997).
[19] V. Haddadi-Asl, M. Kazacos, M. Skyllas-Kazacos, J. Appl. Polym. Sci. 57 (1995) 1455–1463.
[20] Ch.M. Hagg, M. Skyllas-Kazacos, J. Appl. Electrochem. 32 (2002) 1063–1069.
[21] B.C.H. Steele, A. Heinzel, Nature 414 (2001) 345–352.
[22] D.D.L. Chung, J. Mater. Eng. Perform. 9 (2) (2000) 161–163.
[23] C. Randy, D.D.L. Chung, Carbon 40 (2002) 2285–2289.
[24] M.S. Yazici, D. Krassowski, J. Prakash, J. Power Sources 141 (2005) 171–176.
[25] H. Tawfik, Y. Hung, D. Mahajan, J. Power Sources 163 (2007) 755–767.
[26] M.S. Lee, L.J. Chen, Z.R. He, et al., J. fuel cell Sci. Technol. 2 (1) (2005) 14–19.
[27] P. Zhao, H. Zhang, H. Zhou, B. Yi, Electrochim. Acta 51 (2005) 1091–1098.
[28] A. Heinzel, F. Mahlendorf, O. Niemzig, et al., J. Power Sources 131 (2004) 35–40.